EFDA–JET–PR(12)11

B. Cannas, A. Fanni, A. Murari, A. Pau, G.Sias
and JET EFDA contributors

Manifold Learning to Interpret JET High-Dimensional Operational Space

Manifold Learning to Interpret JET High-Dimensional Operational Space

B. Cannas[1], A. Fanni[1], A. Murari[2], A. Pau[1], G.Sias[1]
and JET EFDA contributors*

JET-EFDA, Culham Science Centre, OX14 3DB, Abingdon, UK

[1]Electrical and Electronic Engineering Dept. - University of Cagliari, Italy
[2]Consorzio RFX-Associazione EURATOM ENEA per la Fusione, I-35127 Padova, Italy
** See annex of F. Romanelli et al, "Overview of JET Results",*
(23rd IAEA Fusion Energy Conference, Daejon, Republic of Korea (2010)).

Preprint of Paper to be submitted for publication in
Plasma Physics and Controlled Fusion

ABSTRACT.
In this paper, the problem of visualization and exploration of JET high-dimensional operational space is considered. The data comes from plasma discharges selected from JET campaigns from C15 (year 2005) and up to C27 (year 2009). The aim is to learn the possible manifold structure embedded in the data, to create some representations of the plasma parameters on low-dimensional maps, which are understandable and which preserve the essential properties owned by the original data.

A crucial issue for the design of such mappings is the quality of the data set. This paper reports the details of the criteria used to properly select the more suitable signals downloaded from JET data bases, and the algorithms to pre-process the diagnostic signals in order to obtain a data set of real–time reliable observations. Moreover, a statistical analysis is performed in order to recognize the presence of outliers. Finally, data reduction, based on clustering methods, is performed to select a limited and representative number of samples for the operational space mapping.

Among the large number of manifold learning methods, in this paper three have been investigated: two linear algorithms (Principal Component Analysis and Grand Tour) and one non linear (Self Organizing Maps). The obtained maps can be used to identify characteristic regions of the plasma scenario, allowing to discriminate between the regions with high risk of disruption and those with low risk of disruption.

1. INTRODUCTION

Tokamak is the most promising device for nuclear fusion. The range of 'plasma states' accessible in a Tokamak is highly restricted by disruptive events: plasma instabilities, usually oscillatory modes, sometimes grow and cause abrupt ejection of energy from the plasma and the premature termination of the discharge .

Disruptions are able to cause considerable damage, especially in larger tokamaks like JET or ITER. Hence one of the most challenging problems in nuclear fusion research consists of understanding disruptive events.

One possible way to increase the knowledge on disruptive events consists of identifying characteristic regions in the parameter operational space where the plasma undergoes a disruption and of identifying the operational boundaries of the disruption-free plasma parameter space. However, the huge quantity and high-dimensionality of diagnostic signals that can be regarded as disruption precursors and plasma state variables pose significant challenges to the comprehension of the information hidden in the data.

Nevertheless, even if the data is embedded in a high D-dimensional space, this does not necessarily imply that its actual dimensionality of the phenomenon is D. Assuming that the data of interest lies on an embedded, possibly non-linear, manifold within the higher-dimensional space, the curse-of-dimensionality can be avoided and the data can be represented well in a low-dimensional subspace. To this purpose, recently, dimensionality reduction and manifold learning methods have been actively investigated [1]. Among the simpler linear methods we can cite Principal Component Analysis (PCA) [2], whereas among non linear methods one of the most popular is the Self Organizing Mapping

(SOM) [3] and its probabilistic variant, the Generative Topographic Mapping [4]. Grand Tour (GT) has been proposed [5] to examine structure of high dimensional data using dynamic graphics.

In the past, empirical explorations of the operational boundaries of a tokamak and of the theoretical stability limits of the plasma were performed in order to determine the disruption-free operational space: the Greenwald plasma density limit [6], the high-β limit [7], the li–qψ diagram [8] and the ratio of the radiated power to the input power [9]. Nevertheless, none of them led to the development of a reliable predictive model of disruptions. Moreover, all these contributions are limited to analyze two plasma parameters at a time.

In [10] a statistical analysis of disruptions at JET has been presented, showing the so-called Hugill-diagram [11] for the operations of JET between 2000 and 2007. The statistics for all operations has been given with respect to two plasma parameters: a normalized plasma density, and the inverse of the safety factor. The disruptivity diagram is also reported versus the same parameters, which is a measure for the likelihood that a disruption takes place when the plasma is in a specific state. Similar diagrams have been reported showing the statistics with respect to other two plasma parameters. Even if the analysis performed by De Vries [10] gives very useful information on the disruptivity over a long period of JET operations, it could not be always sufficient to plot disruptivity as a function of only two parameters, because the causes that lead up to a disruption can be due to a complex mixture of events.

A viable approach to better understand these complex events consists of identifying and explaining the intrinsic structure of the data used to describe the plasma operational space, such as neighborhood relationship, global distribution and clustering. Identifying intrinsic structures is the essence of exploratory data analysis and visualization.

Only few attempts have been performed in the past to map the tokamak multidimensional operational space. In particular, in [12] the ASDEX Upgrade tokamak high-dimensional operational space is mapped into lower-dimensional maps using two clustering techniques, K-means and Self-Organizing Maps. Thanks to the reduction in the data dimensionality, the obtained maps allow visualizing different regions of the operational space, clearly highlighting the presence of a large safe region formed by safe plasma states and a smaller disruptive region formed by disruptive plasma states. A transition region, where safe and disruptive plasma states coexist, appears as a boundary between the safe and the disruptive regions. In [13] the 2-dimensional SOM of the 7-dimensional plasma parameter space of ASDEX Upgrade has been used as a disruption predictor by analyzing the trajectories described over the map by the discharges under test. The prediction performance of the system, evaluated on a set of discharges different from those used for the map training, are quite good, with an average success rate of 87%.

In [14] a first attempt to use Generative Topographic Maps to map the JET operational space represented by the temporal evolution of 13 signals is performed. The proposed technique allows observing different clusters in the data at different times before the disruption. The transition between clear separation and overlap of the points in the selected feature space corresponds to the interval [200, 180] ms before the disruption.

In the present paper, the problem of visualization and exploration of the high-dimensional JET operational space has been tackled using three manifold learning methods: PCA, GT, and SOM. The data comes from non disruptive and disruptive discharges selected from JET campaigns from C15 (2005) to C27 (2009), corresponding to the shot interval 63718 – 79853. The aim is to learn the possible manifold structure embedded in the data to create some representations of the plasma parameters on low-dimensional maps, which are understandable and which preserve the essential properties owned by the original data.

Criteria and algorithms have been developed in order to select a set of reliable real time signals to be used as representation of the disruptive and non disruptive JET operational space. For computational reasons, data reduction, based on clustering methods, has to be performed to select a limited and representative number of samples for the mapping.

The maps make use of a set of 10 plasma parameters: plasma current, poloidal beta, Mode Lock amplitude, safety factor at 95% of major radius, total input power, plasma internal inductance, plasma centroid vertical position, line integrated plasma density, stored diamagnetic energy time derivatives, and total radiated power.

The reduction of 10-dimensional data to 2-or 3-dimensional space and the grouping of similar data items together, allows one the visualization of the plasma parameter space and the extraction of useful information on characteristic regions of the plasma operational space and on their associated risk of disruption.

2. MANIFOLD LEARNING

Scientists often deal with problems involving high-dimensional data. The most obvious issue is the visualization; when the data dimension is greater than three they cannot be visualized and it becomes harder to perceive similarities and dissimilarities between different variables. Furthermore, the sampling of the space is harder due to the high number of possible data samples. Essentially, the amount of data to achieve a given spatial density of data increases exponentially with the dimensionality of data space (empty space phenomenon).

In absence of simplification assumptions, algorithms that operate on high-dimensional data are faced with the "curse of dimensionality" and the associated issues, resulting in a very high time complexity. For example, many machine learning algorithms slow down and get stuck in local minima. Reducing data to fewer dimensions often makes analysis algorithms more efficient and can help machine learning algorithms make more accurate predictions.

One approach to simplification is to assume that the data of interest lies on a low-dimensional manifold, embedded in the high-dimensional space. Thus, data reduced to a small enough number of dimensions can be visualized in the low dimensional embedding space. Attempting to uncover this manifold structure in a data set is referred to as manifold learning.

In the last few years, many manifold learning techniques have been developed for dimensionality reduction. A number of supervised and unsupervised linear dimensionality reduction frameworks have been designed [1], which define specific procedures to choose interesting linear projections

of the data. In this paper, Principal Component Analysis [2] and Grand Tour [5] have been tested to reduce the dimensionality of JET data. These linear methods can be powerful, but often miss important nonlinear structure in the data.

Recently, several different algorithms have been developed to perform dimensionality reduction of low-dimensional nonlinear manifolds [1]. Among them, in this paper Self Organizing Maps (SOMs) [3] potentiality has been investigated to map JET operational space.

Let us consider the problem of reducing the dimensionality of a given data set consisting of high-dimensional points in Euclidean space. The high-dimensional input points will be referred to as $X = \{x_1, x_2, \ldots x_N\}$ with $x_i \in \Re^n$. Let k be the dimensionality of the manifold that the input is assumed to lie on. The low-dimensional representations that the dimensionality reduction algorithms find will be referred to as $Y = \{y_1, y_2, \ldots, y_N\}$ with $y_i \in \Re^n$.

The most popular algorithm for linear dimensionality reduction is Principal Components Analysis. The manifold learning algorithms may be viewed as non-linear analogs to PCA.

2.1. PRINCIPAL COMPONENT ANALYSIS

PCA finds the k directions (vectors) along which the data has maximum variance and the relative importance of these directions. If data lies perfectly along an embedding subspace of $\Re^k$, PCA will reveal that subspace; otherwise, PCA will introduce some errors.

Let the first k principal components of X be $B = [b_1, \ldots b_k] \in \mathbb{R}^{n \times k}$. The columns of B are the directions of maximum variation within the data, and they form an orthonormal basis that spans the principal subspace so there is no redundant information.

The data x_i can be approximated by linear combination of the principal components as

$$y_i = BB^T x_i$$

where $y_i = B^T x_i = c_i$ are the linear coefficients obtained by projecting the training data onto the principal subspace; that is,

$$C = [c_1, c_2, \ldots, c_N] = B^T x_i$$

Despite PCA's popularity it presents a number of limitations. The main drawback is the requirement that the data lies on a linear subspace. Indeed, when data lies in a low-dimensional manifold, not in a low dimensional subspace, PCA does not correctly extract the low-dimensional structure.

Manifold learning algorithms essentially attempt to duplicate the behavior of PCA, but on manifolds instead of linear subspaces.

2.2. GRAND TOUR

The Grand Tour (GT) method, introduced by Asimov [5] and Buja and Asimov [15], is a multivariate visualization method that generates a continuous sequence of low dimensional projections of a high dimensional data set. The animation obtained provides an overview of the high dimensional space in a sequence of 2D plots. Data are looked from all possible viewpoints to get an idea of the overall distribution.

To create a two dimensional Grand Tour, a sequence of planes is generated. The set of planes

has to be dense in the data space; the sequence of planes is also required to move continuously from one plane to the next so that the human visual system can smoothly interpolate the data and track individual points and structures in the data. Hence the mathematics of the Asimov-Buja Grand Tour requires a continuous, space-filling path through the set of planes in the high-dimensional data space. Then data has to be projected onto the planes and observed in a time-sequenced set of 2D images. Several algorithms have been proposed to achieve these two conditions, based on obtaining a general rotation in the high dimensional space.

In this paper the MATLAB implementation in [16] of the Pseudo Grand Tour algorithm, firstly described in Wegman and Shen [17], has been used. The main advantages of the Pseudo Grand Tour, that is an approximate version of the Grand Tour, are speed, ease of calculation, uniformity of the tour, and ease of recovering the projection. However, the algorithm is not space filling, thus only a "pseudo" grand tour is obtained.

2.3. SELF ORGANIZING MAP

The Self Organizing Map is a type of Artificial Neural Network developed by Kohonen [3]. SOMs are widely applied as nonlinear dimensionality-reduction tools in order to convert complex nonlinear relationship between data items into a low dimensional space. A SOM replaces a set of points in the D-dimensional input space X onto a smaller set of points **w**, called prototypes, in a low-dimensional regular lattice with a predefined topology. It can be considered as a nonlinear version of PCA as it replaces PCA plane with an articulated grid and fit the grid through the data cloud.

Thus, SOM simultaneously performs the combination of two concurrent subtasks: vector quantization and dimensionality reduction.

Moreover, SOM preserves the topological properties of the input. This means that points close to each other in the input space are mapped on the same or neighbouring prototypes in the embedding space. Preserving neighborhood's relations in the mapping makes possible to see more clearly the structure hidden in the high-dimensional data.

The prototypes have coordinates in the initial space as well as in the embedding space. Coordinates in the embedding space are known before running the SOM because they are fixed in the lattice. On the other hand, the corresponding coordinates in the data space are unknown and are determined during the SOM training. Once these coordinates are computed, each data point is represented as the coordinates associated with the nearest prototype in the data space.

The coordinates **w** are initialized and then updated iteratively during the SOM training procedure. The SOM runs through the data set X several times, called epochs. During each epoch, for each xi, the closest prototype vector wr is determined. Then, the coordinates of all the prototypes are updated according to the learning rule

$$w_i = \eta\Lambda(i, r)(w_i - w_r)$$

The neighbourhood function $\Lambda(i, r)$ is equal to 1 for $i = r$, and falls off exponentially with the distance

d_{ir} between prototypes i and r in the lattice. Thus, prototypes close to the winner r, as well as the winner itself, have their coordinates updated, while those further away, experience little effect.

When the training is completed, the prototypes define the partitioning of the multidimensional data.

Learning generally proceeds in two broad stages: a shorter initial training phase, in which the map reflects the coarser and more general patterns in the data, followed by a much longer fine tuning stage, in which the local details of the organisation are refined. We start with a wide range of $\Lambda(i, r)$ and η and then reduce both the range of $\Lambda(i, r)$ and the value of η gradually as learning proceeds. A typical choice for $\Lambda(i, r)$ is

$$\Lambda(i, r) = e^{-d_{ir}^2/2\sigma^2}$$

where σ is a width parameter that is gradually decreased.

3. THE DATA BASE

The database has been built taking into account a set of signals recorded by several diagnostics and available from JET experimental campaigns. For the selection of the signals to be considered, an analysis based on physical considerations and the availability in real time has been done, also with reference to the plasma parameters used from various authors for disruption prediction both on JET [18] and ASDEX Upgrade (AUG) [19]. The selected signals are representative of the behavior of both the plasma "safe" configurations, i.e. when the pulses are correctly terminated, and when a disruption occurs. Thus, the database contains both *safe* and *disruptive* pulses, which have been classified making reference mainly to the main JET disruption database. Discharges for which the plasma current remained below 1MA were discarded as for disruptive events these are usually insignificant at JET.

The parameters considered to build the database are available in real time in the JET Pulse File (JPF) system or can be directly calculated by other signals available in real time. The set of considered signals is shown in Table 1.

Among all the pulses available from JET campaigns, only those belonging to the campaigns from *C15* to *C27* have been taken into account, because, during the shutdown following the campaign *C14*, changes were made to in-vessel components such as divertor tiles during this period. In the aforementioned interval, *10366* pulses have been selected, including safe and disruptive shots, for which all the signals in Table 1 are available from diagnostics in real time [20]. According to the literature [18], in order to synchronize the signals on the same time base vector, a sampling frequency of $1kHz$ has been chosen.

Some of the chosen signals are described in the following, making reference to those which required assumptions or processing, pointing out the most important characteristics from the statistical and the physical point of view.

a) The Poloidal beta is calculated as $\beta_p = \frac{3}{2}\frac{1}{A}\int_V pdV$ where p is the plasma pressure, V is the

plasma volume, and $A = \frac{1}{4}\,\mu_0 R^* I_p^2$ is a normalizing factor that can be calculated in different ways as reported in [21]. Here, R^* can be assumed equal to 2.96m, according to the JET XLOC definition, or to the geometric major radius of the plasma according to the JET EFIT definition.

b) The internal inductance l_i is defined in the Shafranov equations [22] and it may be written in non-dimensional form as $l_i = \frac{1}{A}\int_V \frac{B_t^2}{2\mu_0}\, pdV$, where B_t is the toroidal magnetic field.

c) In this paper, the safety factor q_{95}, at the 95% flux-surface radius, has been recalculated using the following expression: $q_{95} = \frac{B_t \cdot a^2 k}{2RI_p \cdot 10^{-7}}$ [11], that is a cylindrical approximation for the safety factor. Here, R is the major radius of the plasma, a is the minor radius, and k is the elongation of the plasma shape. All the parameters in the formula are available in real time. Recalculation is needed as the q_{95} signal, available from the diagnostic in real time, besides being affected by noise, offsets and outliers, as many of the other selected plasma parameters, in many cases is not even consistent with the time evolution of the signals from which it depends.

d) The plasma density nelid is the line integrated density, and it is available in real time.

The present database has been built with the main purpose to obtain a mapping of the machine operational space of JET flat-top phase of the discharges. In this paper, only the non intentional disruptions have been taken into account. In the campaigns *C15 - C27*, 428 non intentional disruptions are retained, for which all the 10 signals reported in Table 1 result to be available [23].

A statistical analysis has been performed in order to identify eventual anomalous signals and a not negligible number has been found to be unusable because of the excessive presence of outliers or a time evolution with no physical meaning, probably due to a fault of the correspondent diagnostic during the acquisition.

Such a selection has given rise to a final dataset of 243 non intentional disruptions.

By analyzing the distributions of the signal values, a proper range of variation for each signal has been assumed to clean the data. These ranges have been validated with the help of JET physicists.

A time instant $t_{pre\text{-}disr}$ has to be defined for the disrupted discharges, which discriminates between the non disruptive and the disruptive phase. Because reconstructing the length of disruptive phase from unreliable or unavailable disruption precursor signals for each discharge could be a time consuming solution at JET, in this paper $t_{pre\text{-}disr}$ has been assumed equal for all the discharges, and it has been set following some suggestions reported in literature. In fact, as suggested in [24] and [14], in general disruptions manifest themselves clearly only with a maximum notice of about $180 \div 200$ms.

Hence, the dataset for each disruptive pulse consists of the 10 signals made of 210 points each (one sample every 1ms), in the time interval $[t_D - 210 \div t_D]ms$, where t_D is the time in which the disruption takes place.

The main statistical parameters of the cleaned data in the time interval $[t_D - 210 \div t_D]ms$ have

been reported in Table 2.

Then, confidence limits at 1% and 99% has been used for each signal through the quantile function. The introduction of a confidence level is widely employed as reported in the literature [25]. Regarding the utilization of confidence level it is very important to point out that pratically all the thresholds for cleaning the data have been chosen with consistent margin with respect to the real limit values of the signals. The final number of disruptive samples is 50151.

3.1 SAFE DISCHARGES

In the considered interval of campaigns (*C15 - C27*), all the *10* signals included in Table 1 are available for *10366* safe discharges. The pulses for which the plasma current is less than 1MA have been discarded obtaining 9000 safe discharges.

Moreover, all the pulses for which the signals to be used are not consistent, from a physical point of view or in relation to a suitable range of values, have been discarded.

Being each signal sampled at $1kHz$, a huge amount of data is available for describing the safe operational space. A first shot selection has been performed taking into account that several shots are repeated with similar settings of the parameters. This analysis has been based on various statistical parameters (mean, median, minimum, maximum and standard deviation of each signal for all the pulses), and the resulting selection has been widely validated by visual inspection. Finally 1467 safe discharges are retained, which results in more than $20M$ samples. Note that, this number is too large to be handled by the data visualization algorithms. Furthermore, it is much larger than the number of disrupted samples, for which only the last 210ms are considered. For this reason, data reduction has to be performed on the safe samples in order to obtain a balanced data set. First of all, as for disruptive shots, a data cleaning has been performed discarding the outliers.

Then, the k-means clustering technique [26] has been employed as a base for the development of the data reduction algorithm. The application of the k-means algorithm requires the normalization of data in order to maximize the effectiveness of the clustering. Here, the variables have been normalized between 0 and 1.

For each pulse, the samples are grouped in a fixed number of clusters. Such a number has been chosen by optimizing the value of a clustering validation index (the *Dunn Index* [27]) for a limited number of pulses. Here, 10 clusters have been used; note that by increasing such number, no performance improvement is reached while a greater computational burden ensues. Then, in each cluster, the samples are selected in such a way to maximize the inter-distance among them. For this purpose, *10*-dimensional bubbles, spaced each other with a regular step and centered in the centroid of each cluster, are exploited to pick up a set of samples that are representative of the entire cluster and reflect the information of the starting data in terms of mapped space, even if with a lower density of samples. The implemented algorithm is parameterized with respect to the data reduction ratio. In this paper, a ratio of 1/70 is set.

In Figure 1, the result obtained by the data reduction algorithm for the Pulse No: 66389 is visualized through a PCA projection. Figures 1(a) and (b) show the two principal components of

the 10-dimensional samples before and after data reduction, respectively.

Besides the visual investigation, for evaluating the goodness of the algorithm, the distributions of the original and reduced datasets have been evaluated showing that they are comparable.

The data reduction algorithm allows one to reduce the original database from $20M$ to about $0.3M$ samples.

The main statistical parameters for the cleaned data of the selected safe pulses have been reported in Table 3.

Also here, confidence limits at 1% and 99% has been used for each signal, leading to about 240000 samples.

4. MAPPING OF THE JET OPERATIONAL SPACE

In order to explore the structure of the 10-dimensional JET operational space, graphical methods and manifolds learning algorithms have been applied: Grand Tour, PCA, and SOM.

As the range of variation of the signals is very different, even several orders of magnitude, and since the manifold learning algorithms make use of space metrics, scaling of variables is mandatory. Hence, before projecting data, each signal in the data base has been normalized between 0 and 1 by using the min-max normalization.

Further knowledge can be added to the intrinsic knowledge contained by the 10-D data associating a label to each sample in the data set: a safe state is associated to each non disruptive sample, whereas a disruptive state is associated to each disruptive sample.

4.1 GRAND TOUR

To get an idea of the distribution of the 10-D JET data, a sequence of 2D images has been generated using Grand Tour algorithm. Figure 2 shows four 2-D scatterplots corresponding to different iterations of the algorithm, i.e. to different viewpoints, where blue points correspond to safe samples whereas red points correspond to disruptive samples. As can be noted, safe regions (blue) and disrupted regions (red) can be identified, even if overlaps are present.

4.2 PRINCIPAL COMPONENT ANALYSIS

One of the mostly used dimensionality reduction methods is the Principal Component Analysis [2]. PCA performs an orthogonal linear transformation of the components of the original input data in such a way that they are uncorrelated one with each other.

In this paper, the resulting principal components have been ordered and the first two (2-D visualization) or three (3-D visualization) components are used as new coordinate axes. In this way, the components that contribute more to the variation in the dataset are retained. The Dimensionality Reduction Toolbox of Matlab [28] has been used.

Figure 3 shows the projection of the JET data onto the first two principal components. Here too, blue points correspond to safe samples whereas red points correspond to disruptive samples. On the left hand side of the figure, the safe points have been plotted before the disruptive ones,

conversely on the right hand side the disruptive points have been plotted before the safe ones. As it can be noted, with this representation, two principal components are not enough to clearly separate the disruptive operational space from the safe one.

The 10-D training samples have been also projected on the first three principal components, giving a 3-D visualization of the operational space of JET. Figure 4 reports the 3-D PCA projection. The visualization power of this map is higher than the previous one. However, some overlapping is still present.

Note that PCA performs a linear transformation of the input variables; in order to handle and discover nonlinear relationships between variables, a nonlinear algorithm for dimensionality reduction could be more effective .

4.3 SELF ORGANIZING MAP

The SOM is a non-linear dimensionality reduction method that produces a low-dimensional map of data by preserving their topology. The map consists of components called node or clusters. First of all, the map dimension, i.e., the number of clusters in the SOM has to be properly selected. This has been done optimizing some performance indexes commonly used in literature to evaluate how appropriate the clustering, performed by the SOM, is [29]. Moreover, limiting the number of clusters preserves the generalization capability of the map. It is mandatory to choose the map dimension to maximize its capacity to discriminate among patterns with different features, keeping in the meanwhile a high generalization capability. A good tradeoff between these requirements is achieved with 4998 clusters.

The resulting map has 10 input neurons and 4998 neurons in the 2-D Kohonen layer. In this paper, the SOM Toolbox 2.0 for Matlab [29] has been used to train the SOM. The safe or disruptive label associated to each sample can be used to identify four main categories of clusters in the SOM, depending on their composition: empty clusters, which contain no samples; disruptive clusters, which contain disruptive samples; safe clusters, which contain safe samples; mixed clusters, which contain both safe and disruptive samples.

A color has been associated to each cluster of the map, depending on its class membership (see Figure 5): safe clusters are blue; disruptive clusters are red, mixed clusters are grey, and empty clusters are white. Each color, which is representative of a particular cluster composition, corresponds to a different disruption risk.

The 2-D SOM in Figure 5 clearly highlights the presence of a large safe region (blue) with an associated low risk of disruption, some disruptive regions (red), with a high risk of disruption well separated from the safe region by transition and empty regions. Therefore, safe and disruptive states of plasma seem quite well separated in the SOM.

In Figure 6 the SOM composition in terms of clusters (Figure 6.a) and samples into the clusters (Figure 6.b) is reported. The color code is the same used in Figure 5.

As it can be seen, 73.45% of the clusters are safe clusters that contains 59% of the total samples, that are more than 68% of the safe ones. The disruptive region contains about 6% of the total samples,

that are more than 52% of the disruptive ones. Moreover, 14.53% of the clusters are mixed clusters that contains 33.58% of the total samples, i.e. the transition regions contain 93635 samples; more than 80% of them being safe samples.

One of the causes of the presence of transition clusters is the choice of a unique value of $t_{pre\text{-}disr}$ for all the discharges. This choice is due to the lack of information on the length of the pre-disruptive phase for each shot, and can lead to incorrectly label some samples of disruptive discharges or to miss some information.

Further effort has to be devoted in order to reduce the transition region and better define the boundary between safe and disruptive regions. Note that the coordinates of the prototypes are known in the original multidimensional space, allowing identifying the values of plasma parameters along the boundaries between safe and disruption regions.

Some tools are available to analyze the SOM results. One of them is the Component Plane [30]. This tool allows a global view of the database and supports the user in detecting if there is any relation between variables. The Component Plane representation expresses the relative component distributions of the input data on the 2D map. The dependencies between different variables can be identified by comparing the corresponding component planes: similar patterns (the colors corresponding to the values of the variables) in identical locations on the component planes are consistent with correlated components. In Figure 7 (a-h) the component planes for I_p, β_p, LM, q_{95}, P_{tot}, l_i, ne_{lid}, and P_{rad} are shown. Figure 7 highlights that the high disruption risk regions in the top-right corner and in the right side of the SOM in Figure 5 correspond to a combination of high values of LM, q_{95}, and l_i, and to low values of Ip. Moreover, by picking a same cluster in each plane (in the same location), we could assemble the relative values of the plasma parameters of the cluster prototypes. Another possible representation is the D-Matrix, whose elements correspond to the clusters of the SOM. The D-matrix visualizes the median distance between a cluster and adjacent clusters. Thus, it allows one to display the similarity of data elements into one cluster with respect to the data into nearest clusters. With this representation, it is possible to detect if there are macro-clusters of data and to judge if eventually they are well separated or not. In Figure 8, the D-Matrix corresponding to the SOM in Figure 5 is shown. Light areas, where the distances between clusters are minimal, can be thought as macro-clusters and dark areas as separators. The high disruption risk regions in the top-right corner and in the right side of the SOM in Figure 5 are well identified in the same location in Figure 8. Other separated regions can be identified in the bottom of the D-Matrix display, which does not correspond to further high disruption risk regions. Nevertheless, the component planes of β_p, P_{tot}, li, ne_{lid}, and P_{rad} clearly show that the bottom region of map correspond to modifications in the operational parameters of the machine.

In literature, several efforts have been done to define a relationship between disruption risk and operational ranges. The most common diagrams concerning the tokamak operational ranges are related to the low-q and density limit (Hugill diagram), and to the β-limit.

The Hugill diagram shows the operational ranges with respect to the low-q limit and the density limit. The boundary of operation as limited by disruptions is plotted against the inverse edge safety

factor $1/q$ and the Murakami parameter $n_e \cdot R/B_t$, where n_e is the line averaged plasma density (in m^{-3}). Disruptions generally restricts operation to a region $q > 2$ and to electron density such that $(n_e \cdot R/B_t) \cdot q$ is below a critical value in the range $10 \div 20 \cdot 10^{19}$ $m^{-2}T^{-1}$ or higher when additional heating is applied [11]. At JET, a critical value of $40 \cdot 10^{19}$ $m^{-2}T^{-1}$ independent of the power has been empirically found as shown in [10].

Figure 9(a) shows the Hugill diagram for the safe samples, whereas Figure 9(b) shows the same Hugill diagram for the disruptive samples. Darker colors correspond to regions with high data concentration, as quantified in logarithmic scale by the color bar. An off-line signal for the line averaged density is available, even if for a limited number of the discharges considered in our data base.

All the safe data lies in the region where $(n_e \cdot R/B_t) \cdot q_{95} < 40 \cdot 10^{19}$ and $q_{95} > 2$. Few disruptive samples exceed the Greenwald limit, as shown in literature [9]. As can be noted from the Hugill diagrams, several plasma configurations, leading to disruptions in less than 210ms, are positioned in the same region of the safe discharges, confirming that a 2D representation is not suitable to distinguish between regions with high risk of disruption, and those with low risk of disruption.

Another operational limit is the β-limit. Usually, tokamaks operate under the levels of $\beta_N = \beta_t \cdot (a \cdot B_t/I_p) = 4 \cdot l_i$ where β_N is the normalized β and β_t is the toroidal β.

Figure 10 (a) and (b) report data belonging to SOM's safe and disruptive clusters respectively, in the plane β_t (%) versus $l_i \cdot I_p / (a \cdot B_t)$; the β–limit is given by the black line. As it can be noted, the β–limit does not appear on these graphs since both configurations lie in the region below the black line. This is mainly because no real high β disruptions seem to have happened during the considered period, as shown in [10]. Moreover, the operational space is more complex, hence, it is not possible to distinguish safe and disruptive configurations looking at their position in the diagram, as highlighted also in [23].

These results point out the effective visualization capabilities of SOMs for extracting valuable information from a large amount of high-dimensional data.

CONCLUSIONS

This paper aims to test the data visualization capability of some manifold learning algorithms as tools to analyse and understand the high dimensional operational space of JET.

Firstly, a database of disruptive and safe shots has been built: some statistical analyses have been carried out on the available shots, in order to exclude shots containing corrupted diagnostic signals and those not holding all prescribed signals. Moreover, some pre-processing algorithms have been applied on selected plasma parameters in order to obtain reliable data. Finally, data reduction, based on clustering methods, has been performed to select a limited and representative number of samples for the operational space mapping.

The resulting database contains samples coming from 1467 safe and 243 disruptive discharges belonging to the range 63718–79853 in the experimental campaigns from *C15* to *C27*.
Three manifold learning methods have been investigated (Grand Tour, Principal Component

Analysis, and Self Organizing Maps) to map the JET high dimensional operational space in lower dimensional spaces. The results show the superiority of SOM to identify characteristic regions of the plasma scenario, allowing to detect the regions with high risk of disruption, and those with low risk of disruption.

The comparison of 2D SOM data representation with traditional 2D representations such as the Hugill diagram and the β_t versus $l_i \cdot I_p/(a \cdot B_t)$ diagram highlights the efficiency of the SOM both for data visualization and understanding of the high dimensional plasma parameter space.

In future work, for disruption prediction purposes, the data visualization capability of the SOM map could be exploited in order to monitor the discharge evolution, by tracking on the map the plasma trajectory during the experiment. The results obtained at ASDEX Upgrade [13] are encouraging.

ACKNOWLEDGEMENT

This work was supported in part by the Italian MIUR (research program PRIN 2008) and by the Euratom Communities under the contract of Association between EURATOM/ENEA. The views and opinions expressed herein do not necessarily reflect those of the European Commission.

REFERENCES

[1]. J. A. Lee, M. Verleysen (2007). Non linear Dimensionality Reduction, Springer.

[2]. Jolliffe, I. T. (1986). Principal Component Analysis. Springer-Verlag, 487.

[3]. Kohonen MT (1989) Self-Organization and Associative Memory. Springer-Verlag, New York.

[4]. Bishop, C., Svensén, M., & Williams, C. (1998). GTM: The generative topographic mapping. Neural Computation, **10**(1), 215–234.

[5]. Asimov D. (1985). The Grand Tour: a Tool for Viewing Multidimensional Data. SIAM Journal on Scientific and Statistical Computing, **6**(1):128- 143, 1985.

[6]. Greenwald M. (2002). Density Limits in Toroidal Plasmas Plasma Physics and Controlled Fusion **44** 27–80.

[7]. Murakami M. et al (1976). Some observation on maximum density in tokamaks experiments Nuclear Fusion **16** 347–8.

[8]. Fielding S.J et al (1977). High-density discharges with gettered torus walls in DITE Nuclear Fusion **17** 1382–5.

[9]. Wars D.J. and Wesson L.A. (1992). Impurity influx model of fast tokamaks disruptions Nuclear Fusion **32** 1117–23.

[10]. De Vries, M.F. Johnson, I. Segui and JET EFDA Contributors (2009) Statistical analysis of disruptions in JET Nuclear Fusion **49** 055011 (12pp)

[11]. Wesson J. (2004). Tokamak 4th edition (Oxford: Clarendon)

[12]. M. Camplani, B. Cannas, A. Fanni, G. Pautasso, G.Sias, P. Sonato, and the Asdex-Upgrade Team(2011). Tracking of the Plasma States in a Nuclear Fusion Device using SOMs Neural Computing and Applications: **20**, 6, 851-863.

[13]. R. Aledda, B. Cannas, A. Fanni, G. Pautasso, G. Sias (2012) Mapping of the ASDEX

UPGRADE operational space for disruption prediction IEEE Transactions on Plasma Science, Vol. **40**, no.3, pp. 570 - 576, DOI: 10.1109/TPS.2011.2174385.

[14]. G.A. Rattá, J. Vega, A. Murari, M. Johnson and JET EFDA contributors, "Disruption Prediction at JET with a Combination of Exploratory Data Analysis and Supervised Methods," n Proceedings of the HTPD High Temperature Plasma Diagnostic 2008, Albuquerque, New Mexico. (11th May 2008 - 15th May 2008).

[15]. A. Buja and D. Asimov (1986). Grand Tour Methods: An Outline. In D.M. Allen, editor, Computer Science and Statistics: Proc. of the 17th Symposium on the Interface, pages 63-67, Amsterdam: North Holland, Elsevier Science Publisher B.V.

[16]. Martinez, W.L., Martinez, A.R. (2005). Exploratory data analysis with MATLAB, CHAPMAN & HALL/CRC, A CRC Press Company, Boca Raton London New York Washington, D.C..

[17]. Wegman, E. J., and Shen, J. (1993), "Three-Dimensional Andrews Plots and the Grand Tour," in: Tarter, M. E., and Lock, M. D. (Eds.), Computing Science and Statistics: Proceedings of the 25th Symposium on the Interface, Interface Foundation of North America: Fairfax Station, VA, 284-288.

[18]. G.A. Rattá, J. Vega, A. Murari, G. Vagliasindi, M.F. Johnson, P.C. de Vries, and EFDA-JET Contributors (2010). An advanced disruption predictor for JET tested in a simulated real-time environment Nuclear Fusion **50**, 025005 (pp.10).

[19]. Y. Zhang, G. Pautasso, O. Kardaun, G. Tardini, X.D. Zhang and the ASDEX Upgrade Team (2011). Prediction of ASDEX Upgrade disruptions using discriminant analysis Nuclear Fusion, 51, 063039 (12pp).

[20]. "Real Time Data Network" (2008). http://users.jet.efda.org/rtmcwiki/images/0/0e/Rtdn-data.pdf.

[21]. S. N. Gerasimov, T. C. Hender, M. F. Johnson, L. E. Zakharov and JET EFDA contributors, 37th EPS Conference on Plasma Physics, Dublin, Ireland, 21-25 June 2010, P4.121 (European Physical Society, 2010) Conference Proceedings.

[22]. Shafranov V.D. (1971). Determination of the parameters and in tokamak for arbitrary shape of plasma pinch cross-section Plasma Physics, **13**, n.9, 757-762.

[23]. P.C. deVries et al (2011) Survey of Disruption Causes at JET, Nuclear Fusion **51** 053018 (12pp).

[24]. A. Murari, J. Vega, G.A. Rattà, G. Vagliasindi, M.F. Johnson, S.H. Hong and JET-EFDA Contributors (2009). Unbiased and non-supervised learning methods for disruption prediction at JET Nuclear Fusion **49** 055028 (11pp).

[25]. Cox D.R., Hinkley D.V. (1974) Theoretical Statistics, Chapman & Hall.

[26]. Lloyd S P (1982) Least squares quantization in PCM IEEE Transaction on Information Theory **2** 129-137.

[27]. Dunn J (1974). Well separated clusters and optimal fuzzy partitions. J Cybern (4) 95–104.

[28]. Matlab Toolbox for Dimensionality Reduction (v0.7.2 - November 2010).

[29]. SOMtoolbox, Adaptive Informatics Research Centre, Helsinky Univ. of Technology, Finland. http://www.cis.hut.fi/projects/somtoolbox/, 2005.

[30]. J. Vesanto, et al., 2000 SOM toolbox for Matlab5, Helsinki Univ. of Tech., http://www.cis.hut.fi/somtoolbox/package/papers/techrep.pdf

JPF Signals	Acronym	Unit
Plasma Current	I_p	A
Poloidal Beta	β_p	a.u.
Mode Lock Amplitude	LM	V
Safety Factor at Major Radius	q_{95}	a.u.
Total Input Power	P_{tot}	W
Plasma Internal Inductance	li	a.u.
Plasma Centroid Vertical Position	Z_{cc}	m
Line Integrated Plasma Density	ne_{lid}	m^{-2}
Stored Diamagnetic Energy Time Derivative	W_{dia}	W/s
Total Radiated Power	P_{rad}	W

Table 1: Set of considered signals.

SIGNAL	MIN	MAX	MEAN	MEDIAN	STD
I_p	7.00E+005	3.85E+006	1.86E+006	1.87E+006	4.08E+005
β_p	3.03E-006	3.16E+000	3.17E-001	2.07E-001	3.41E-001
LM	1.00E-004	4.65E-003	5.58E-004	4.55E-004	3.97E-004
q_{95}	2.02E+000	9.66E+000	4.01E+000	3.80E+000	1.06E+000
P_{tot}	1.46E+005	4.04E+007	5.76E+006	3.48E+006	5.77E+006
li	3.62E-001	2.60E+000	1.09E+000	1.12E+000	1.78E-001
Z_{cc}	1.26E-003	1.17E+000	2.71E-001	2.76E-001	6.75E-002
ne_{lid}	4.02E+018	2.68E+021	1.02E+020	7.47E+019	1.73E+020
W_{dia}	-2.39E+007	1.19E+007	-1.09E+006	-7.45E+005	1.91E+006
P_{rad}	1.01E+005	1.99E+008	4.83E+006	2.76E+006	8.75E+006

Table 2: Non intentional disruptions statistics ($t_D - 210 \div t_D$]ms)

SIGNAL	MIN	MAX	MEAN	MEDIAN	STD
I_p	8.16E+05	3.86E+06	2.03E+06	1.96E+06	3.12E+05
β_p	6.47E-06	2.95E+00	3.10E-01	1.92E-01	2.70E-01
LM	1.00E-04	5.00E-03	2.16E-04	2.06E-04	9.18E-05
q_{95}	2.33E+00	7.49E+00	3.89E+00	3.81E+00	6.86E-01
P_{tot}	1.00E+05	3.26E+07	4.33E+06	1.42E+06	5.30E+06
li	5.87E-01	2.40E+00	1.06E+00	1.11E+00	1.16E-01
Z_{cc}	1.39E-01	4.71E-01	2.91E-01	3.00E-01	3.66E-02
ne_{lid}	4.01E+18	4.80E+20	6.71E+19	5.10E+19	4.35E+19
W_{dia}	-2.40E+07	2.52E+07	2.37E+04	2.36E+04	9.27E+05
P_{rad}	1.00E+05	9.96E+07	2.47E+06	6.10E+05	6.39E+06

Table 3: Safe discharges statistics

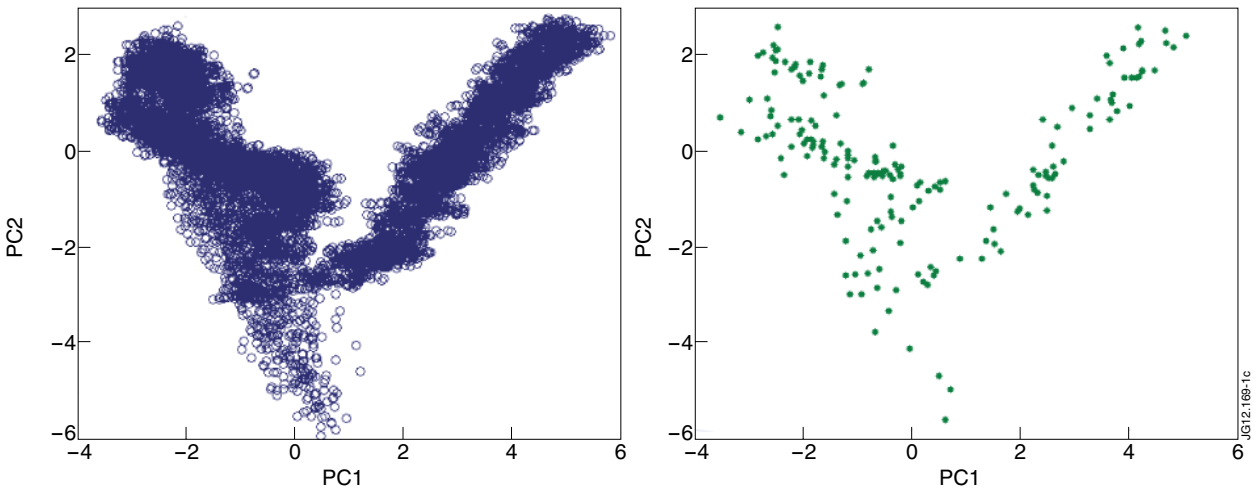

Figure 1: Result of the data reduction algorithm visualized through PCA (Pulse No: 66389): scatter plot of the first two PCs (a) of the dataset; (b) of the dataset after data reduction by k-means.

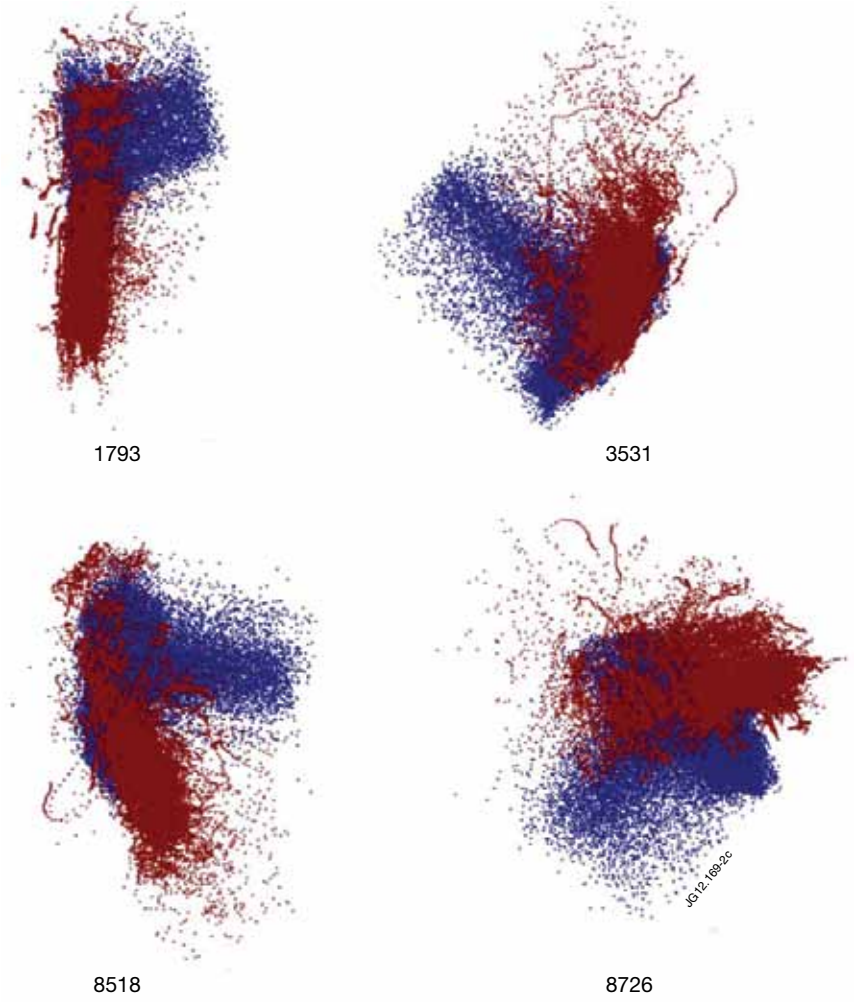

Figure 2: Grand Tour projections of 10-D training disruptive (red) and safe (blue) samples at different iterations.

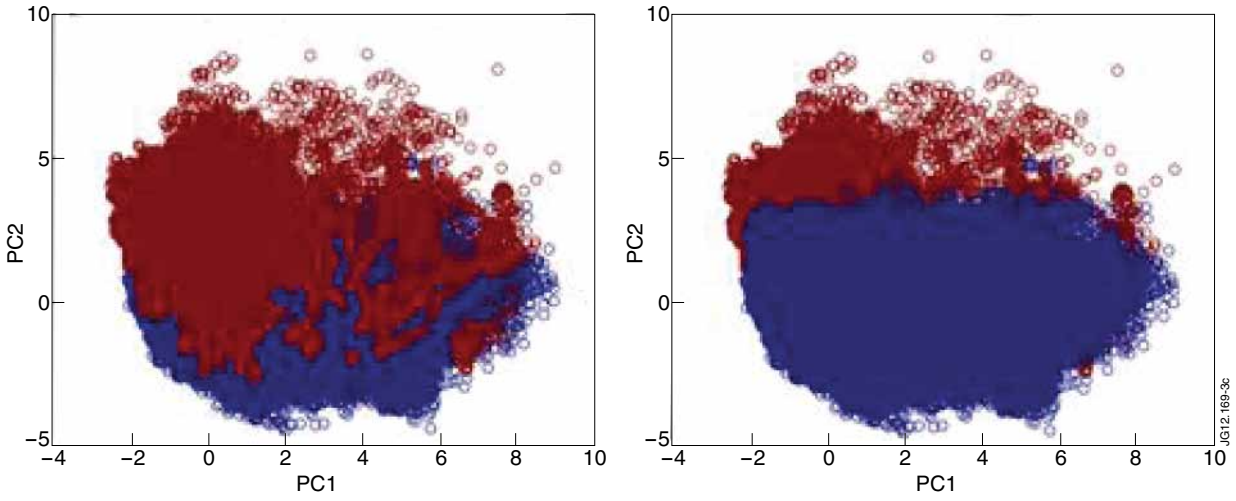

Figure 3: PCA projection of the 10-D training samples on the 2-D PCA; safe samples (blue), disruptive samples (red).

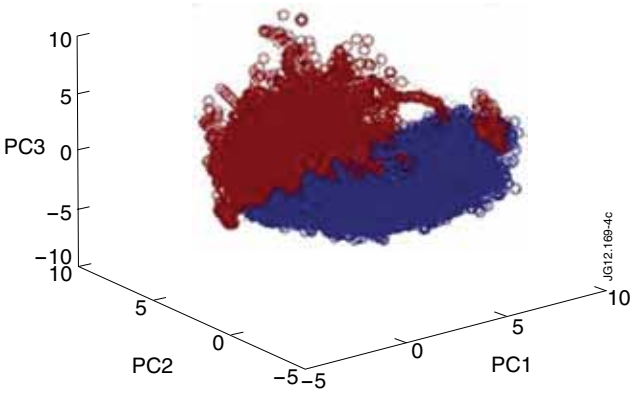

Figure 4: PCA projection of the 10-D training samples on the 3-D PCA; safe samples (blue), disruptive samples (red).

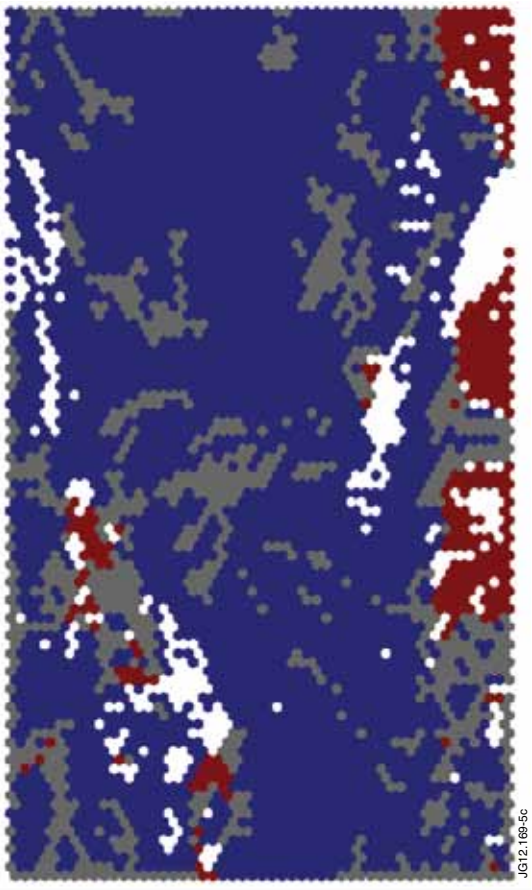

Figure 5: 2-D SOM of the 10-D JET operational space: safe clusters (blue), disruptive clusters (red), mixed clusters (grey), empty clusters (white).

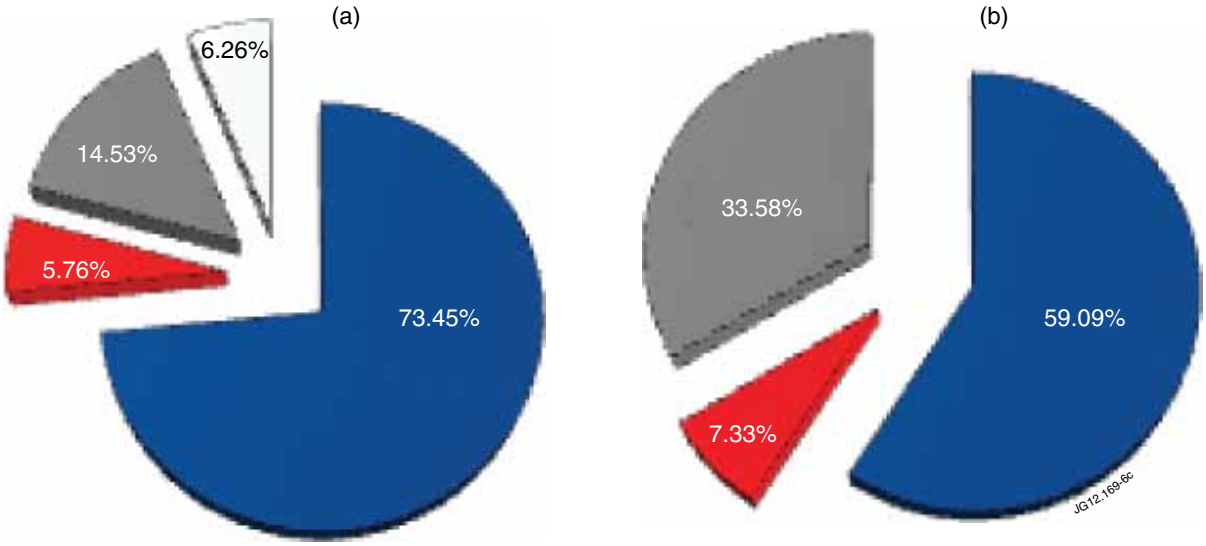

Figure 6: Composition of the SOM in Figure 5 in terms of: (a) clusters; (b) samples into the clusters. Safe clusters/samples (blue), disruptive clusters/samples (red), mixed clusters/samples (grey), empty clusters (white).

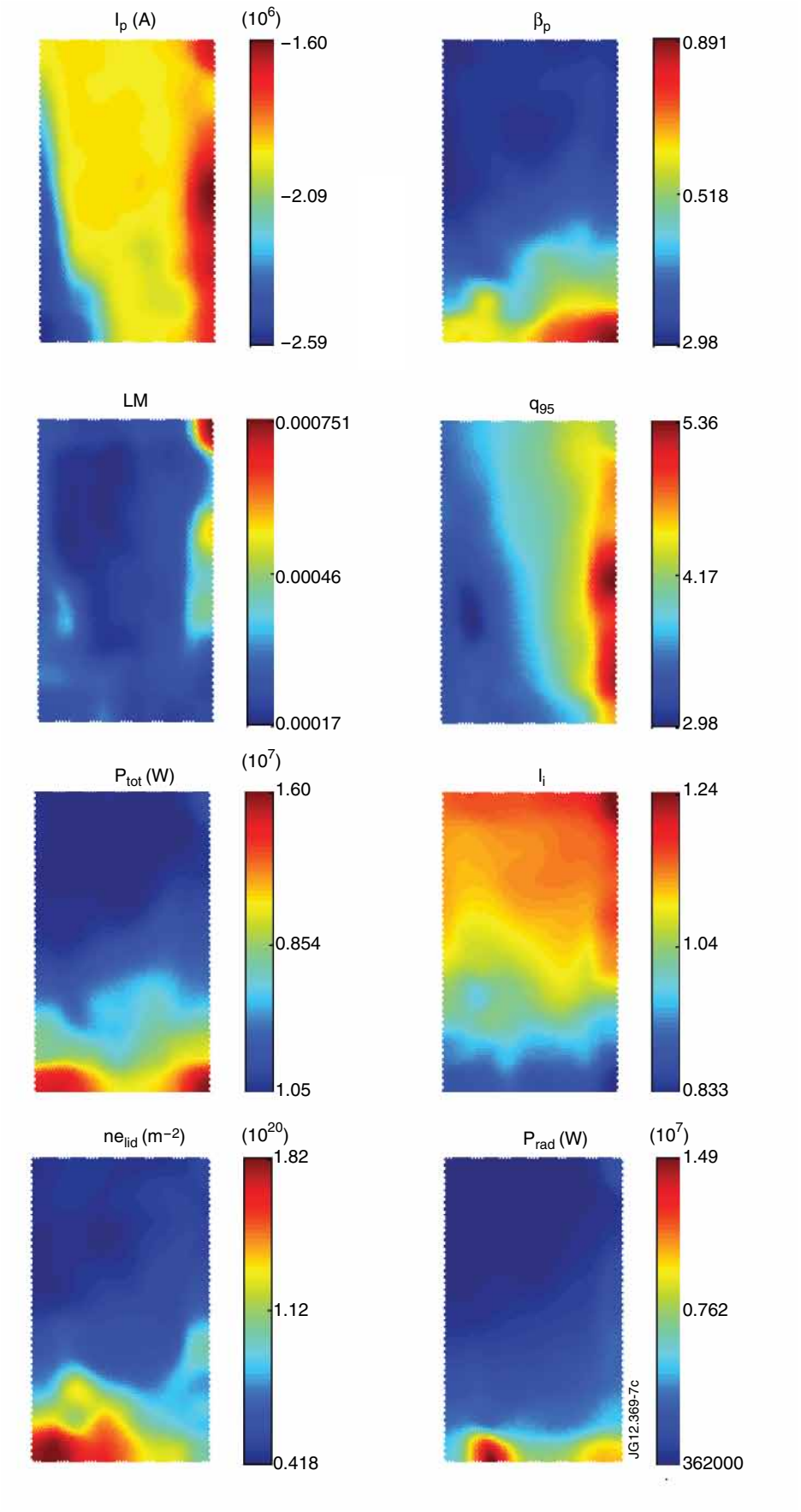

Figure 7: Component plane representation for I_p, β_p, LM, q_{95}, P_{tot}, l_i, ne_{lid} and P_{rad}.

Figure 8: SOM: D-Matrix

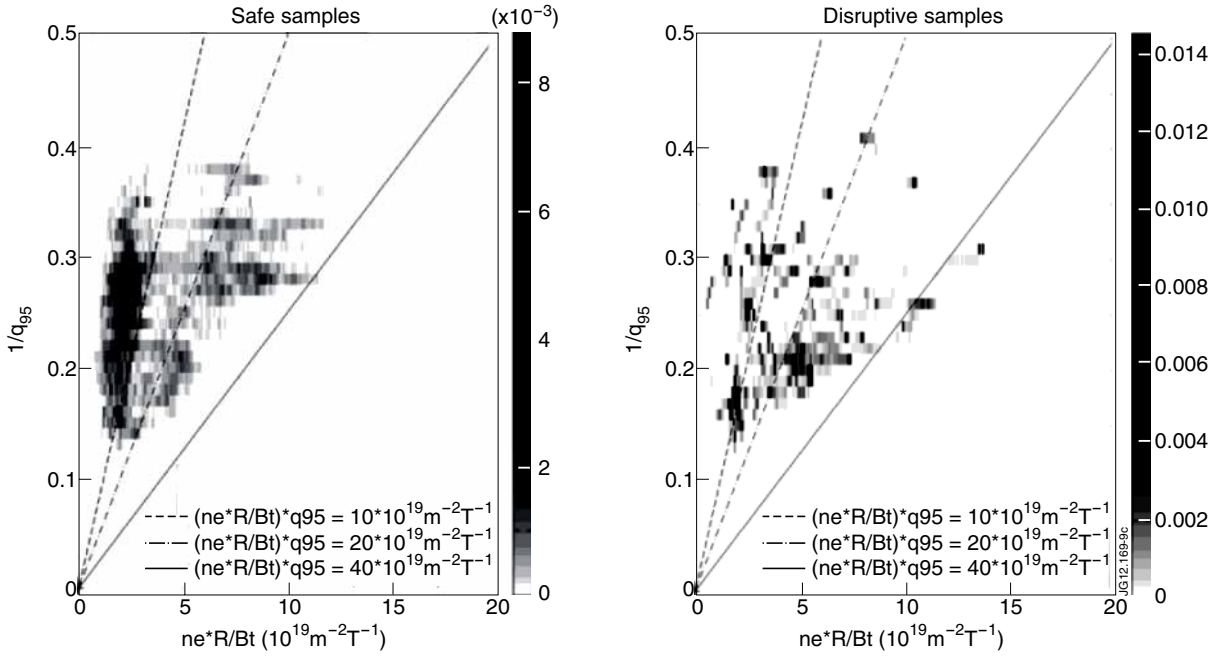

Figure 9: Hugill Diagram showing the operating regime for: (a) safe discharges; (b) last 210 ms of disruptive discharges

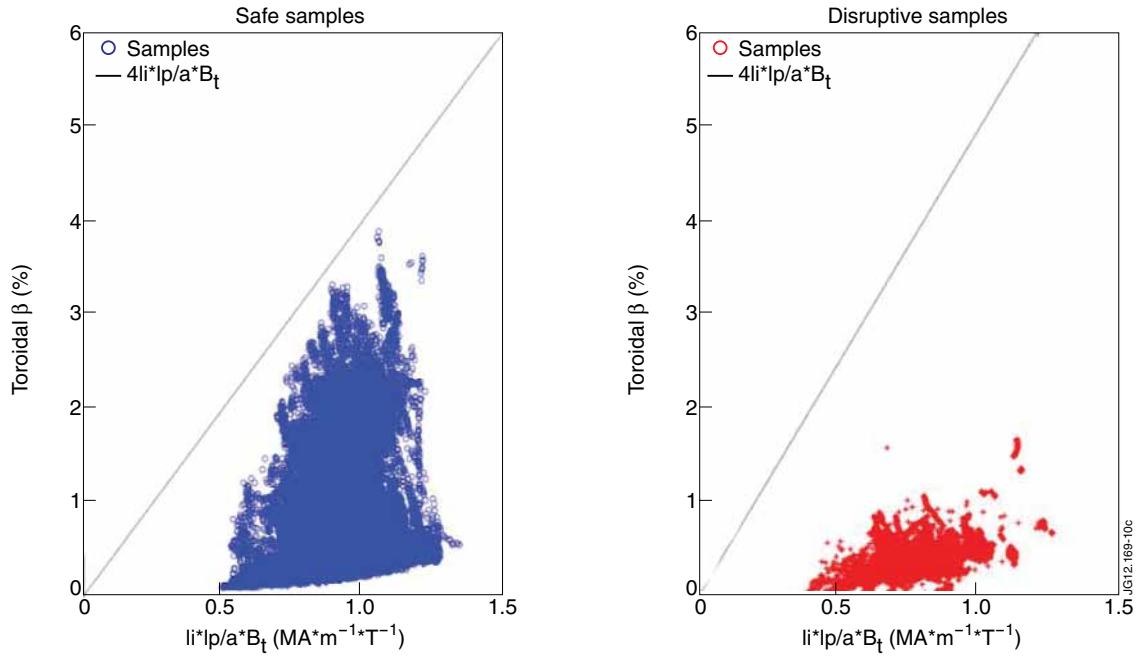

Figure 10:Scatter plot of the toroidal β_t (%) versus $l_i I_p/aB_t$: (a) samples in the safe SOM clusters; (b) samples in the disruptive SOM clusters.